ISSN 2007-9737

Camera as Position Sensor for a Ball and Beam Control System

Alejandro-Israel Barranco-Gutiérrez[1,3], Jesús Sandoval-Galarza[2], Saúl Martínez-Díaz[2]

[1] Tecnológico Nacional de México, Instituto Tecnológico de Celaya, Mexico

[2] Tecnológico Nacional de México, Instituto Tecnológico de La Paz, Mexico

[3] Cátedras CONACyT, Mexico

israel.barranco@itcelaya.edu.mx, {jsandoval, saulmd}@itlp.edu.mx

Abstract. This paper describes a novel strategy to use a digital camera as a position sensor to control a ball and beam system. A linear control law is used to position the ball at the desired location on the beam. The experiments show how this method controls the positioning of the ball in any location on the beam using a camera with a sampling rate of 30 frames per second (fps), and these results are compared with those obtained by using an analog resistive sensor with a feedback signal sampled at a rate of 1000 samples per second. The mechanical characteristics of this ball and beam system are used to simplify the calculation of the ball position using our vision system, and to ease camera calibration with respect to the ball and beam system. Our proposal uses a circularity feature of blobs in a binary image, instead of the classic correlation or Hough transform techniques for ball tracking. The main control system is implemented in Simulink with Real Time Workshop (RTW) and vision processing with OpenCV libraries.

Keywords. Computer vision, ball and beam system, linear control.

1 Introduction

Currently, vision-based feedback is used in many modern control systems. One advantage of this is the fact that cameras provide measurement information without contact, eliminating friction. In addition, a computer vision system allows more generalization, as it facilitates the identification of different objects from images, for example, cars, blood cell position, color of liquids, facial expressions, and movement of people or stars. Hence, vision-based control system research is important to improve the performance of its applications.

P. Corked suggests a general visual control framework [1, 2] describing the flow of information between the blocks of this type of systems. This is represented in a hierarchical diagram of modules in a robot-vision system showed in Fig. 1. Visual servoing considers environment as images that

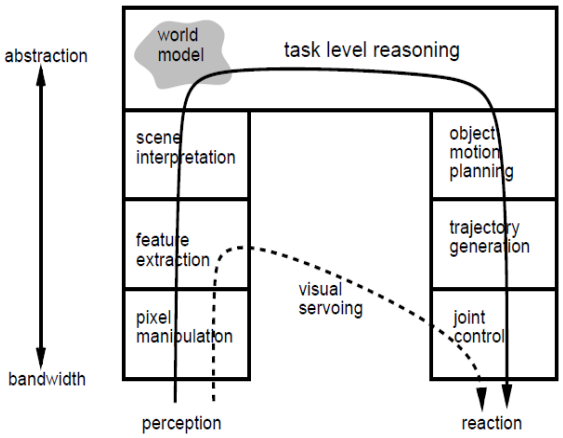

Fig. 1. General structure of a hierarchical model-based robot and vision system

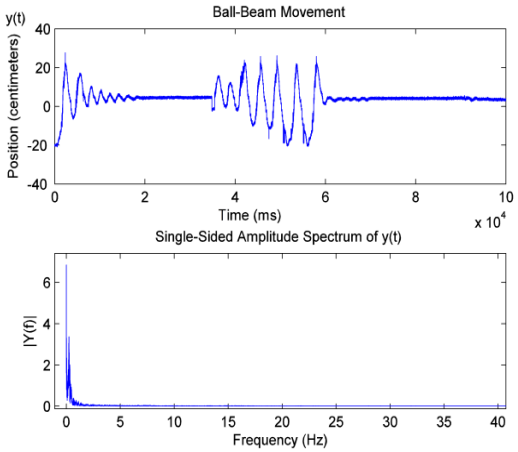

Fig. 2. Ball movement signal in time and frequency domains

react controlling the actuators (joins) with respect to a reference signal. Interpretation of the scene and task-level reasoning images are considered more abstract tasks. This work is a particular case of visual servoing represented by the dashed line in Fig. 1.

The main disadvantage of visual control is a low speed response of conventional cameras, typically around 30 fps [3]. In this context, an experimental analysis was realized to determine the bandwidth of the ball movement in frequency domain. According to the above, we can implement a real time system based on the definitions in the Nyquist sampling theorem [4]. Fig. 2 shows the signal frequency spectrum $Y(\omega)$ of the ball movement $y(t)$ in real conditions, where ω is the angular frecuency in radians and t is the time in milliseconds. The signal's energy is located within the frequency range from 0 to 2 Hz; thus, we consider a minimum sampling period of 500 milliseconds.

There have been several contributions from other similar ball and beam systems: in [5] the beam angle is measured with a vision-based method, while in [6] the ball position is determined with two cameras, with the intention of placing the ball only in the center of the beam. Other proposals use neural networks and/or fuzzy logic for feeding signals to the PID controller, with a visual ball and beam control using correlation-based tracking algorithms [7]. In this work we describe in detail the performance of a camera as a position sensor, supplying the information of the ball's position on the beam in a linear control system without any camera delay compensation, showing explicitly the behavior of the visual ball detection and location. The ball can be positioned on the beam at any place within the range from -15 cm to 15 cm as experiments illustrate. Other important aspects are the low complexity for ball detection with scale invariance and easy camera calibration with respect to the ball and beam system. The latter allows variable distance between the camera and the mechanism. In summary, our main contribution is a novel scheme to control a ball and beam system using a camera as a ball position sensor. The proposed ball and beam visual control system is composed by the following subsystems:

– Vision System,
– Real Time Control System,

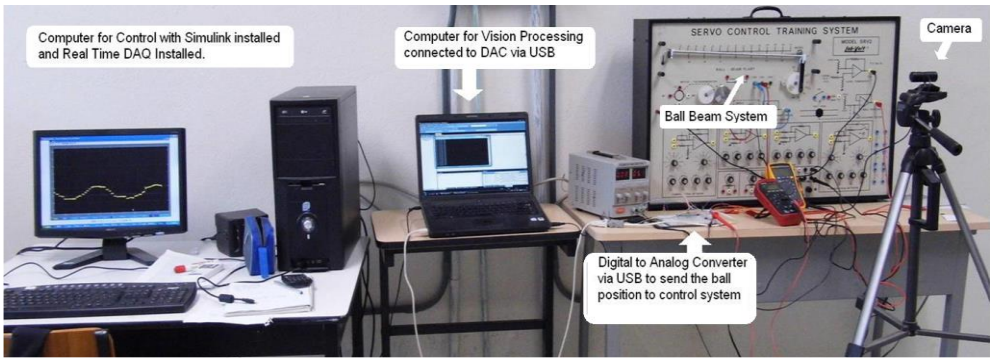

Fig. 3. Experimental configuration of vision sensing for the ball and beam control system

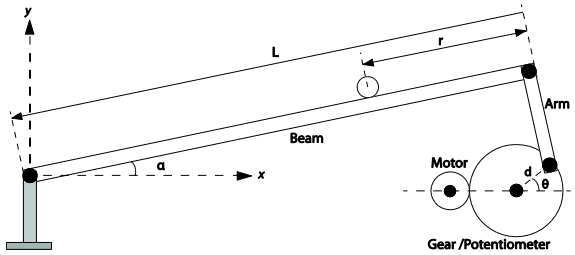

Fig. 4. The ball and beam system

– Ball and Beam System (BBS),
– Vision-Control Interface.

With respect to the hardware, the visual system is connected to the control system in terms of voltage; accordingly, the vision system and the analogous sensor send the same type of information. The control law considers two loops: the first is the motor position that moves the beam, and the second loop detects the ball and provides its position with respect to the center of the beam which is driven horizontally. The left side of the beam (from 0 to 15 cm) is considered positive and the right side (from 0 to -15 cm) is considered negative for ball position. The ball location is communicated to the control system which acts on the motor as a response of the control law. Typically, the position of the ball is measured using a special sensor (of analog type), which acts as a potentiometer and works as a voltage divisor; the sensor provides a voltage level when the ball remains in any position on the beam. In our proposal, a camera replaces the analog sensor, while conserving the voltage relationship of the analog sensor (see Fig. 3).

2 The Ball and Beam System (BBS)

The BBS is an underactuated mechanical system that consists of a steel ball moving along a beam, Fig. 4. One side of the beam is fixed, while the other side is coupled with a metal arm attached to a gear, manipulated by means of an electric motor such that the beam can be controlled by applying an electrical control signal to the motor. The absence of actuation in the ball determines the underactuated nature of the mechanism. A schematic picture of the BBS is shown in Fig. 4, where r and α are the linear position of the ball and the angle of the beam, respectively. The length of the beam is given by L, d and θ are the radius and angle of the gear/potentiometer, respectively.

2.1 Dynamic Model

An idealized mathematical model that characterizes the behavior of a permanent-magnet DC motor controlled by the armature voltage is typically described by the set of equations [8]:

$$v = R_a i_a + L_a \frac{di_a}{dt} + e_b, \tag{1}$$

$$e_b = k_b \theta_m, \tag{2}$$

$$\theta_m = N\theta, \tag{3}$$

$$\tau_m = k_a i_a, \tag{4}$$

where

v: Armature (V),
R_a: Armature resistance (Ω),
i_a: Armature current (A),
L_a: Armature inductance (H),
$\mathrm{e_b}$: Back electromotive force (V),
$\mathrm{k_b}$: Back electromotive force constant (V·s/rad),
θ_m: Angular position of the axis of the motor (rad),
N: Gears reduction ratio,
θ: Angular position of final gear (rad),
τ_m: Torque at the axis of the motor (N·m),
$\mathrm{k_a}$: Motor-torque constant (N·m/A).

Appendix A describes the procedure used to obtain the following transfer functions for this BBS:

$$P_1(s) = \frac{\theta(s)}{v(s)} = \frac{18.7}{s(s+11)}\left(\frac{\mathrm{rad}}{\mathrm{V}}\right), \tag{5}$$

$$P_2(s) = \frac{r(s)}{\theta(s)} = \frac{0.438}{s^2}\left(\frac{\mathrm{m}}{\mathrm{rad}}\right). \tag{6}$$

2.2 Linear Control Law

A block diagram that relates the desired linear position $\mathrm{r_d}$ to the linear position r of the ball is

shown in Fig. 5, where we have included $G_1(s)$ and $G_2(s)$ as the blocks of the controllers.

In Fig. 5, $k_1 = k_3 = 0.247$ (V/m) and $k_2 = 1.6$ (V/rad) are conversion factors verified experimentally. We have used the classical control theory to design a linear control law. Specifically, we apply a proportional control to the internal loop (beam position) with $G_2(s) = k_p = 3.7$. Also, taking into account the structure of a lead compensator

$$G_c(s) = k_c \frac{(s+\frac{1}{T})}{(s+\frac{1}{\alpha T})}, \quad (7)$$

where $0 < \alpha < 1$, we designed the following lead compensator to external loop (ball position)

$$G_1(s) = \frac{6(s+1)}{s+11}, \quad (8)$$

with stability margins of 50º (phase margin) and 9 dB (magnitude margin).

3 Ball Visual Detection and Location

The main considerations in achieving ball visual detection and location are low computational costs, uncontrolled environments, and easy calibration between camera and the BBS. The processing reduction is one of most important aspects of this stage, providing a fast system response and rapid signal analysis of ball movement. In this context, the ball detection is based on circularity, a feature measurement which needs few processing operations to be calculated [9]. The comparison between our proposal and correlation algorithms or Hough Transform [10, 11] shows that our method needs considerably fewer microprocessor instructions and allows a simple calibration process between the camera and the BBS [12, 13]. Because the circularity is invariant to scale, the method has two important advantages: first, the distance between the BBS and the camera could be variable, and second, the background could have non-circular objects. Table 1 shows the computational complexity of different techniques to detect circles and our method which uses circularity as ball detector. We found that even though circularity has the same computational complexity as correlation, it is invariant to scale changes of the ball image, achieving to setup the camera at different distances with respect to the BBS.

Table 1. Ball visual detection performances

Reference	Technique	Computational complexity	Invariance
Shapiro (2001) [14]	Hough T.	$O((m \times n)^{r-2})$ r: each radius	Scale, rotation and translation.
Tsai (2002) [15]	Correlation	$O(m \times n)$	Translation and rotation.
Our proposal	Circularity	$O(m \times n)$	Scale, rotation and translation.

3.1 Ball Visual Detection

The ball visual detection process can be controlled in terms of illumination, color, and distances as it can be seen in other research [5, 6, 7, 16]. On the other hand, our proposed strategy for ball detection has the following stages:

1. Image acquisition,
2. Interest window cutting,
3. Conversion from color image to gray scale image,
4. Thresholding,
5. Image component labeling,
6. Filtering,
7. Circularity calculus,
8. Ball centroid estimation.

First, a color image is received from the camera with resolution $k \times l \times 3$ (k for rows, l for

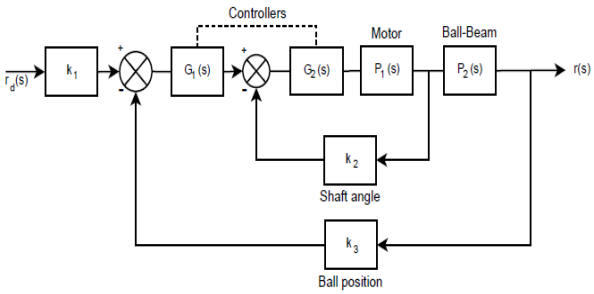

Fig. 5. Block diagram of the control system

columns, and three color components) with 8 bits of resolution for each pixel and RGB color scheme [13] expressed as

$$I(x,y,z) \in \{0 \le \mathbb{Z} \le 255\} \forall \{x | 0 \le x \le k\}, \{y | 0 \le y \le l\}, \{z | 0 \le z \le 2\}, \quad (9)$$

where $I(x,y,z)$ is the RGB image; x,y,z are indexes that locate each pixel, and $\mathbb{Z}$ is the set of integer numbers.

As part of the calibration process, the user selects a rectangular area with two clicks on the left upper corner (i_0, j_0) and the right lower corner (i_1, j_1). The small window selected contains the area in which the ball and the beam appear in the image $I_w(x,y,z)$; this consideration reduces the image processing cost from a $k \times l \times 3$ image to an $(i_1 - i_0) \times (j_1 - j_0) \times 3$ image:

$$I_w(x,y,z) = I(x,y,z), \quad \forall \{i_0 \le x \le i_1, j_0 \le y \le j_1, z\}. \quad (10)$$

We chose not to color the ball to allow a greater generalization in ball detection. The ball material is an opaque metal. This permits the use of an image in gray scale, reducing the computational cost by passing from a $k \times l \times 3$ matrix to another $k \times l \times 1$ matrix. Then, the program converts the image to gray scale:

$$I_g(x,y) = \frac{\left(I_w(x,y,1) + I_w(x,y,2) + I_w(x,y,3)\right)}{3}. \quad (11)$$

Thresholding segments the image to obtain binary images with regions called *blobs*. We used Otsu's method [17] to obtain a threshold level μ_0 and to get a binary version $b(x,y)$ of $I_g(x,y)$ as

$$b(x,y) = \begin{cases} 1 & if \quad I_g(x,y) \ge \mu_{0,} \\ 0 & otherwise. \end{cases} \quad (12)$$

This processing depends directly on the lighting of the location in which the BBS is setup and the object's brightness in the image. The lighting level was tested in different rooms, from 300 to 700 lux, and it was found that the control system works even as the size of regions in $b(x,y)$ changes. One example is depicted in Fig. 6.

In order to get interconnected component labeling and measure its circularity, the iterative method showed in [9] is used to obtain $O_i(x,y)$

Fig. 6. Ball and beam image in binary

from the binary complement of $b_i(x,y)$ with LN number of labeled blobs as

$$O_i(x,y) = labeling(\bar{b}(x,y)), \quad (13)$$

where $O_i \cap O_j \in \phi \; \forall \; j \ne i$, for $i, j = 1, 2, \ldots, LN$.

However, in $b(x,y)$ it is common to find small non-representative blobs, therefore, area filtering is employed for noise reduction. This filter reduces the processing needed in later stages (inside ball detection). Essentially, it counts the number of pixels in each object and removes the objects out of range

$$Of_i(x,y) = \{O_i \; \forall \; a_i \le area(O_i)\}, \quad (14)$$

where a_i is the smallest area for a blob of interest. Considering that the ball is the most circular blob in the image, we compute the circularity of each $Of_i(x,y)$ and choose the nearest to 1 or maximum called $Of_c(x,y)$ [9]:

$$Of_c(x,y) = \underset{i=1,2,\ldots,LN}{\operatorname{argmax}} \left(\frac{4\pi \; area(Of_i)}{perimeter(Of_i)^2} \right). \quad (15)$$

After choosing the $Of_c(x,y)$, its centroid is calculated to estimate the ball position on the image expressed in pixels as

$$P_2 = (x_2, y_2) = \left(\frac{m_{10}}{m_{00}}, \frac{m_{01}}{m_{00}} \right) \quad (16)$$

where

$$m_{pq} = \sum_{x=i_0}^{i_1} \sum_{y=j_0}^{j_1} x^p y^q Of_c(x,y) \quad (17)$$

with $\mathrm{p}, \mathrm{q} = 0,1$.

3.2 Ball Location

The first step in visually controlling the BBS is the camera calibration with respect to the BBS. The literature offers general methods to perform this task, such as those presented in Zhang [18], Zisserman [19], and Barranco [20]. The

architecture of the BBS simplifies some aspects of the PinHole model because only the ball and the beam move on a plane, and the mechanism is fixed with respect to the camera in order to locate the ball on the beam in quantitative terms such that

$$\lambda\tilde{\mathrm{m}} = \mathrm{A}[\mathrm{R}|\mathrm{t}]\tilde{\mathrm{M}}, \tag{18}$$

where $\widetilde{M} \in \mathbb{R}^4$ denotes a 3D point in homogenous coordinates with respect to the object reference system, $\widetilde{m} \in \mathbb{R}^3$ represents a 2D point in the image with respect to the camera coordinate system, λ is a scale factor, $A \in \mathbb{R}^{3\times3}$ is the intrinsic parameters matrix, and $[\mathrm{R}|\mathrm{t}] \in \mathbb{R}^{3\times4}$ is an augmented matrix that contains the rotation matrix R and translation vector t, which relate the camera and object reference systems as details Zhang [18]. Also, it is necessary to estimate the lens distortion, usually modeled as a polynomial centered on the principal point $(\mathrm{u}_0, \mathrm{v}_0)$ to get the corrected coordinates $(\breve{u}, \breve{v})$ of (u, v):

$$\breve{\mathrm{u}} = \mathrm{u} + (\mathrm{u} - \mathrm{u}_0)[\mathrm{k}_1(\mathrm{x}^2 + \mathrm{y}^2) + \mathrm{k}_2(\mathrm{x}^2 + \mathrm{y}^2)^2], \tag{19}$$

$$\breve{\mathrm{v}} = \mathrm{v} + (\mathrm{v} - \mathrm{v}_0)[\mathrm{k}_1(\mathrm{x}^2 + \mathrm{y}^2) + \mathrm{k}_2(\mathrm{x}^2 + \mathrm{y}^2)^2], \tag{20}$$

where k_1, k_2 are the distortion coefficients. We verify in (19) and (20) that for regions near the principal point the distortion is almost null. An assumption is that the camera is placed in front of the ball and beam mechanism; consequently, the image plane and the plane of the beam movement are parallel. Even if the parallelism is not held, the lineal relation is conserved [18, 19]. Then, the ball position can be estimated using the scheme in Fig. 7.

The advantage of this method is that the user needs only to put the camera in front of the mechanism and select two points for calibration. The user selects the center of the beam $P_0 = (x_0, y_0)$ and one of its extremes $P_1 = (x_1, y_1)$, as it is shown in Fig. 8.

The line between $\overline{P_0P_1}$ expresses the relation between the units of the scale and pixels, and is given by

$$\mathrm{y} - \mathrm{y}_0 = \frac{\mathrm{y}_1 - \mathrm{y}_0}{\mathrm{x}_1 - \mathrm{x}_0}(\mathrm{x} - \mathrm{x}_0). \tag{21}$$

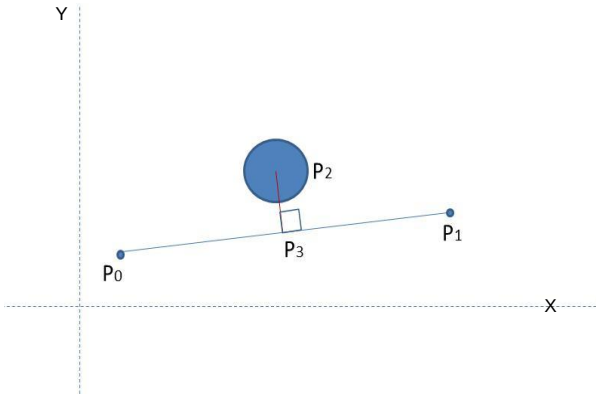

Fig. 7. Ball's position with respect to the beam

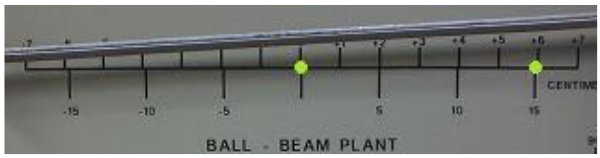

Fig. 8. Scale marked with clear points at 0 and 15 cm

To measure the ball's position we have the following:

$$\mathrm{m}_1\mathrm{m}_2 = -1, \tag{22}$$

$$\mathrm{y} - \mathrm{y}_2 = \frac{\mathrm{x}_0 - \mathrm{x}_1}{\mathrm{y}_1 - \mathrm{y}_0}(\mathrm{x} - \mathrm{x}_2), \tag{23}$$

$$\mathrm{x}_3 = \frac{\mathrm{a}\mathrm{x}_2 - \mathrm{y}_2 - \mathrm{b}\mathrm{x}_0 + \mathrm{y}_0}{\mathrm{a} - \mathrm{b}}, \tag{24}$$

where x_3 is the position of the ball and

$$\mathrm{a} = \frac{\mathrm{x}_0 - \mathrm{x}_1}{\mathrm{y}_1 - \mathrm{y}_0}, \tag{25}$$

$$\mathrm{b} = \frac{\mathrm{y}_1 - \mathrm{y}_0}{\mathrm{x}_1 - \mathrm{x}_0}. \tag{26}$$

To avoid singularities in (21)-(24), the user needs to give click on the center of the beam and its extremes such that $x_0 \neq x_1$ and when $y_0 \neq y_1$ as it is shown in Fig. 7.

Finally, considering that the point $(\bar{x}, \bar{y})$ estimates the value of (x_2, y_2) and based in the previous analysis, we propose the following expression:

$$pos = \left(\frac{a\bar{x} - \bar{y} - bx_0 + y_0}{a - b}\right)\alpha + \beta, \quad (27)$$

where pos is the ball position, α and β are constants to adjust the conversion factors of the analogue sensor and the vision system.

4 Experiments

We used the BBS in order to do experiments. Our benchmark is a servo control training system of Lab-Volt Company, model TM92215, endowed with a permanent-magnet DC motor controlled by the armature voltage and a voltage amplifier, both used to control the BBS. A rotatory potentiometer is used to measure the angular position of the motor sampled at 1000 Hz.

The control algorithm is executed with the same sampling frequency in a PC host computer equipped with the NI PCI-6024E data acquisition board from National Instruments. The camera used in the image acquisition delivers 30 fps with a resolution of 640 x 480 pixels, and a USB interface between the vision system and the control system was used.

We carried out three different experiments to compare the performance of the linear control system when visual and analogous resistive sensors are used. In all experiments, we use the same initial configuration but different desired positions rd (cm). The values to adjust the conversion factors are $\alpha = -0.37$ and $\beta = 173$. The plots are shown in Figures 9-11, where item (a) depicts the time evolution of the ball position when visual sensing is used and item (b) depicts the time evolution of the ball position when resistive sensing is used.

Note that the position vanishes toward the desired position, with a small oscillation. This can be associated with the discretization process of the control plus vision algorithm, the change of the lighting level from 300 to 700 lux, and the absence of delay compensation of visual feedback into the control system.

After observing the results and comparing them to other proposals, we can see that Petrovic [5] does not show the complete behavior of the control system (reference and output signals) in order to evaluate its performance; it only displays

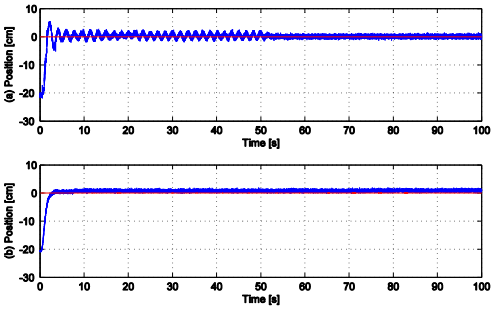

Fig. 9. Time evolution of the ball position with rd=0 cm

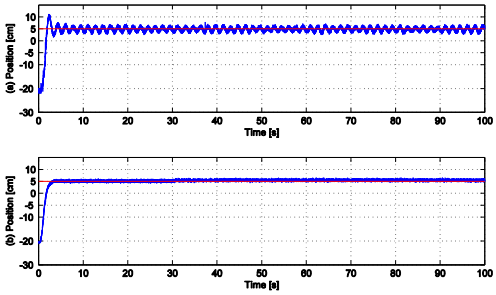

Fig. 10. Time evolution of the ball position with rd=5 cm

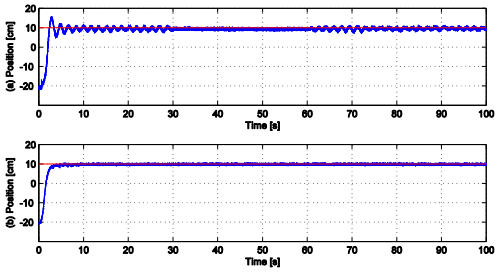

Fig. 11. Time evolution of the ball position with rd=10 cm

the signal delivered by the vision system. Ho [6] proposes to control the BBS using a camera to measure the position of the ball and another to measure the angle of the beam, but can only position the ball in the center of the beam. Xiao Hu [7] uses Fuzzy Logic and Neural Networks to control the system, but the camera calibration in these cases is not as flexible as we propose in this work (giving 2 clicks for calibration and 2 clicks for image processing reduction).

In contrast, our scheme compares the performance when the analog sensor is sampled at 1000 Hz, the camera is at 30 Hz without delay compensation, and the computational complexity with tracking technics is used. It allows to prove the advantages of our scheme.

5 Conclusions

In this paper, we presented a novel scheme for visual control of a ball and beam system. In our scheme, the computational complexity is greatly reduced with the use of circularity feature computation. We replaced the analog resistance sensor with a digital camera, allowing an easy camera calibration and elimination of friction between the sensor and the ball, where the camera uses a sampling frequency of 30 Hz, while the resistive sensor used to measure the linear position of the ball is sampled at 1000 Hz with a data acquisition board.

The calibration method also allows for flexibility in camera positioning in front of the ball and beam mechanism, which only needs four clicks to be configured. We do not compensate for visual processing delay to verify the performance of our proposed scheme.

Acknowledgements

The authors greatly appreciate the support of PROMEP and CONACyT with the project 215435. The work of the second author was partially supported by CONACYT grant 166636 and by TecNM grant 5345.14-P. We would also like to thank Laura Heit for her valuable editorial help.

References

1. **Corke, P. (2011).** *Robotics, vision and control: Fundamental Algorithms in MATLAB.* Springer Verlag.
2. **Corke, P. & Hutchinson, S. (2001).** A new partitioned approach to image based visual servo control. *IEEE Transactions Robot Automation*, Vol. 17, No. 4, pp. 507–515. DOI: 10.1109/70.954764
3. **Handa, A., Newcombe, R. A., Angeli, A., & Davison, A. J. (2012).** Real-time camera tracking: When is high frame-rate best? *Lecture Notes in Computer Science*, Vol. 7578, pp. 222–235. DOI: 10.1007/978-3-642-33786-4_17
4. **Nyquist, H. (1928).** Certain topics in telegraph transmission theory. *American Institute of Electrical Transactions Engineers*, Vol. 47, No. 2, pp. 617–644.
5. **Petrovic, I. (2002).** Machine vision based control of the ball and beam. *IEEE 7th International Workshop on Advanced Motion Control,* pp. 573–577. DOI: 10.1109/AMC.2002.1026984
6. **Ho, C. C. & Shih, C. L. (2008).** Machine vision based tracking control of ball beam system. *Key Engineering Materials,* pp. 301–304. DOI: 10.4028/www.scientific.net/KEM.381-382.301
7. **Xiaohu, L., Yongxin, L., & Haiyan, L. (2011).** Design of ball and beam control system based on machine vision*. Applied mechanics and materials,* Vol. 71-78, pp. 4219–4225. DOI: 10.4028/www.scientific.net/AMM.71-78.4219
8. **Ogata, K. (1970).** *Modern control engineering.* Prentice-Hall.
9. **Sossa, H. (2006).** *Features for object recognition* (in Spanish). Instituto Politécnico Nacional.
10. **Gonzalez, R. & Woods, R. (2008).** *Digital image processing.* Prentice Hall, pp. 201–207.
11. **Barranco, A. & Medel, J. (2011).** Artificial vision and identification for intelligent orientation using a compass. *Revista Facultad de Ingeniería de la Universidad de Antioquía*, Vol. 58, pp. 191–198.
12. **Barranco, A. & Medel, J. (2011).** Automatic object recognition based on dimensional relationships. *Computación y Sistemas*, Vol. 5, No. 2, pp. 267–272.
13. **Voss, K., Marroquin, J. L., Gutierrez, S. J., & Suesse, H. (2006).** *Analysis of images of three-dimensional objects* (in Spanish). Instituto Politécnico Nacional.
14. **Shapiro, L. & Stockman., G. C. (2001).** *Computer Vision*. Prentice-Hall.
15. **Tsai, D. M. & Lin, C. T. (2003).** Fast normalized cross correlation for defect detection. *Pattern Recognition Letters*, Vol. 24, No.15, pp. 2625–2631.
16. **Pérez, C. & Moreno, M. (2009).** *Fuzzy visual control of a nonlinear system.* Master Thesis, Instituto Politécnico Nacional.
17. **Otsu, N. (1979).** A threshold selection method from gray level histograms. *IEEE Transactions on Systems, Man, Cybernetics*, Vol. 9, No.1, pp. 62–66.
18. **Zhang, Z. (2000).** A flexible new technique for camera calibration. *IEEE Transactions on Pattern*

Analysis and Machine Intelligence, Vol. 22, No. 11, pp. 1330–1334. DOI: 10.1109/34.888718

19. **Hartley, R. & Zisserman, A. (2003*).* ***Multiple view geometry in computer vision***. Cambridge University press, pp. 152–208.
20. **Barranco, A. & Medel, J. (2009).** Digital camera calibration analysis using perspective projection matrix. *Proceedings of the 8th WSEAS International Conference on Signal Processing, robotics and automation*, pp. 321–325.

Appendix A

Considering Fig. 4, the equation of motion for this system can be written as

$$J_m\ddot{\theta}_m = \tau_m - B_m\dot{\theta}_m - \frac{\tau}{N}, \tag{28}$$

where J_m is the inertia of the rotor, $B_m$is the viscous friction coefficient of the rotor, and τ is the torque applied after the gear box at the axis of the load such that

$$\tau = J_L\ddot{\theta} + B_L\dot{\theta}, \tag{29}$$

where J_L is the inertia of the load and B_L is the load friction coefficient.

Now, consider a free body analysis with the ball rolling over an inclined plane. Using Newton's law we have

$$m\frac{d^2r}{dt^2} = mg\sin(\alpha) - F, \tag{30}$$

where m is the mass of the ball, g is the acceleration of gravity, and F represents the frictional force parallel to the plane. Our mathematical analysis is done under the following assumptions:

- The ball maintains contact with the plane.
- The magnitude of the moment of the ball is given by $F \cdot r_b$, where F is the force that exerts a moment about the center of mass of the ball, and r_b is the radius of the ball.
- There is no friction between the beam and the ball.

Hence, the rotational equation of the ball becomes

$$I\frac{d^2\phi}{dt^2} = F\, r_b, \tag{31}$$

where I and ϕ represent the inertia moment and the angle of rotation of the ball, respectively. Next, based on the angle of rotation of the ball, we have

$$r = r_b\phi, \tag{32}$$

and considering (31)-(32), we can verify that

$$F = \frac{I}{r_b^2}\frac{d^2r}{dt^2}. \tag{33}$$

Next, if we consider the ball as a uniform sphere, such that

$$I = \frac{2}{5}mr_b^2, \tag{34}$$

and when we substitute (34)-(33) into (30), some algebraic calculus yields

$$\frac{d^2r}{dt^2} = \frac{5}{7}g\sin(\alpha). \tag{35}$$

For small values of α, we assume that $\sin(\alpha) = \alpha$. Therefore,

$$\frac{d^2r}{dt^2} = \frac{5}{7}g\alpha. \tag{36}$$

Using the relationship between the angle gear θ and the beam angle α, we have

$$L\alpha = d\theta, \tag{37}$$

then (36) yields

$$\frac{d^2r}{dt^2} = \frac{5}{7}\frac{d}{L}g\theta. \tag{38}$$

Finally, taking Laplace Transform from (1)-(4), (28), and (38), where we have depicted the inductance of the motor, that is, $L_a = 0$, we obtain the following transfer functions after some algebraic manipulations:

$$P_1(s) = \frac{\theta(s)}{v(s)} = \frac{18.7}{s(s+11)}(\text{rad/V}), \tag{39}$$
$$P_2(s) = \frac{r(s)}{\theta(s)} = \frac{0.438}{s^2}\ (m/rad),$$

where we used the following values: $R_a = 9.6$, $k_b = 5.04\text{x}10^{-3}$, $k_a = 0.0075$, $J_m = 1.76\text{x}10^{-7}$, $B_m = 1.76\text{x}10^{-7}$, $J_L = 7.35\text{x}10^{-3}$, $B_L = 1.6\text{x}10^{-7}$, $L = 0.4064$, $d = 0.0254$, $g = 9.8$ and $N = 75$.

Alejandro-Israel Barranco-Gutiérrez received his B.Sc. degree in Telematics Engineering from UPIITA, as well as his M.Sc. and Ph. D degrees in Advanced Technology from CICATA-Legaria of Instituto Politécnico Nacional, Distrito Federal, Mexico, in 2003, 2006, and 2010, respectively. In 2008, he became professor at the Department of Mechatronics of Instituto Tecnológico de Tláhuac. In 2012 he joined the Computational Systems Master program at Instituto Tecnológico de La Paz as postdoctoral researcher. Since 2014, he has been researcher at Instituto Tecnológico de Celaya. His fields of interest are computer vision, machine learning, and robotics.

Jesús Alberto Sandoval-Galarza was born in Mazatlan, Mexico, in 1971. He received the B.Sc. degree in Electric Engineering from the Instituto Tecnológico de Culiacan, Mexico, and the M. Sc. and Ph. D. degrees in Automatic Control from the Instituto Tecnológico de La Laguna, Mexico and the Universidad Autónoma de Baja California, Mexico, in 1993 and 2010, respectively. He is a professor at the Instituto Tecnológico de La Paz, Mexico. His research interests include automatic control and mechatronics.

Saúl Martínez-Díaz received his M. Sc. degree in Computational Systems from Instituto Tecnológico de La Paz, Mexico, in 2005, and his Ph.D. in Computer Science from Centro de Investigación Científica y de Educación Superior de Ensenada, Mexico, in 2008. He is currently research professor at Instituto Tecnológico de La Paz, Mexico. His research interests include image processing and pattern recognition.

Article received on 22/11/2013; accepted on 09/03/2015.
Corresponding author is Alejandro Israel Barranco Gutiérrez.